Correlation Between Tensile Properties and Network Draw Ratio for Poly(ethylene terephthalate) Fibers with Wide Range of Molecular Orientation and Crystallinity

HIRONOBU SHIRATAKI, AKIKO NAKASHIMA, KAZUISHI SATO, KUNIHIKO OKAJIMA

Fundamental Research Laboratory of Natural & Synthetic Polymers, Asahi Chemical Industry Co., Ltd., 11-7, Hacchonawate Takatsuki, Osaka 569, Japan

Received 31 July 1996; accepted 14 September 1996

ABSTRACT: Poly(ethylene terephthalate) (PET) fibers with wide range of molecular orientation and crystallinity were prepared by the cold drawing of melt-spun yarns in a temperature-controlled water bath and the subsequent annealing for these samples. For all samples, the true stress–strain curves can be principally superimposed to a master curve which corresponds to the stress–strain curve for the original nonoriented amorphous yarn and it was confirmed that the original (intrinsic) network structure is not affected by molecular orientation and crystallinity significantly. Tensile properties of these fibers were studied systematically in terms of the network draw ratio which was determined as a shift factor in the matching process of a true stress–strain curve to the master curve. Consideration of the tensile drawing behavior has shown that the network draw ratio, which is defined as an extension of unique intrinsic network structure, has direct correlation with mechanical properties including the yield and breaking behaviors. When the network draw ratio is taken into consideration, PET fiber, even if it has crystallinity or molecular orientation, has appeared to behave in the manner of an almost ideal rubber during the tensile testing carried out as cold drawing. © 1997 John Wiley & Sons, Inc. J Appl Polym Sci **64:** 2631–2646, 1997

Key words: poly(ethylene terephthalate); network draw ratio; tensile properties; molecular orientation; crystallinity

INTRODUCTION

Poly(ethylene terephthalate) (PET) fibers are quite widely used in various fields, and because of this wide usage, voluminous studies on the mechanical properties of PET fibers have been carried out. As early as 1967, in investigations on the mechanical properties of PET fibers in the cold-drawing behavior, Ward[1] demonstrated that with increase in the molecular orientation expressed by birefringence, the yield stress and initial modulus increase while the ratio of cross-sectional areas before and after neck deformation, i.e., the natural draw ratio, decreases. Based on these results, he concluded that the molecular orientation is the most important factor governing the development of mechanical anisotropy in PET fibers. He also showed that the crystallinity affects the yield mechanism although it has relatively small effect on the initial modulus. Gupta and Kumar[2] and Gupta and Radhakrishnan[3] studied the effect of heat setting on the structure and mechanical properties of PET fiber and showed that the modulus, yield stress, yield strain, and tensile strength have roughly linear relationships with the amorphous orientation factor (fa) estimated from the combination method of birefringence and crystallinity. Rim and Nelson[4] investigated the structure/property rela-

Correspondence to: H. Shirataki.
 CCC 0021-8995/97/132631-16

tions for PET yarns and concluded that the tensile strength, shrinkage, and initial modulus are primarily controlled by amorphous orientation, being higher for higher orientation values.

On the one hand, the effectiveness and usefulness of the concept of network draw ratio has been proved by Long and Ward[5,6] in the studies of tensile-drawing behavior, free shrinkage, and shrinkage force measurements for PET fibers. In their studies, PET fibers were prepared by melt spinning with various take-up speeds to obtain yarns with a wide range of degrees of molecular orientation and, then, those spun yarns were subject to hot drawing over a heated cylinder or hot plate. By discussing the mechanical properties and structure of these fibers in terms of the network draw ratio, they showed that the network draw ratio has a strong correlation with the tensile properties. It follows that the use of a network draw ratio provides a valuable basis on which comparison between the tensile properties and the structure of drawn PET fibers can be made. In their study, however, the possible effects of crystallinity on the network draw ratio have not been discussed in detail.

In this study, we attempted, first, to clarify the effect of molecular orientation and crystallinity of PET fibers on the network draw ratio and, second, to investigate the relationship between the network draw ratio and the mechanical properties such as initial modulus, yield stress, and breaking characteristics for various types of fibers. For these purposes, three types of PET fibers, i.e., oriented amorphous samples, nonoriented crystalline samples, and oriented crystalline samples were prepared to carry out the tensile testing and to determine the network draw ratio. The analysis of mechanical behavior in terms of the network draw ratio for these fibers suggests the existence of an intrinsic network structure of the PET fiber, which is principally preserved during deformation and crystallization.

EXPERIMENTAL

Material

The original undrawn fiber used in this study was prepared by the melt spinning of commercial-grade PET, Bright DEC (Asahi Chemical Ind. Co., Japan) containing 0.06 wt % of TiO_2. The number-average molecular weight of the original polymer before spinning was evaluated as about M_n = 21,000 by the GPC method. In the melt-spinning procedure, a low enough take-up velocity (450 m/min) was used to obtain the original undrawn fiber, which is amorphous in nature without any apparent molecular orientation. The original undrawn fiber thus obtained was approximately 91 μm in diameter and its birefringence Δn was determined as about 1.0×10^{-3} by an interference optical microscope.

Birefringence Measurement

An Interphako microscope (Carl Zeiss Jena) was used to determine the birefringence Δn value of all the samples. In the measurement, a mixed solution of α-bromonaphthalene and olive oil was prepared as soaking media for the measuring sample.

Crystallinity

Wide-angle X-ray diffraction measurements were carried out by an imaging plate-type diffractometer DIP100-S (Mac Science Co., Japan) with a Ni-filtered CuKα radiation X-ray source working at 40 kV, 25 mA. The intensity of the diffracted X-ray at arbitrary points of the scattering angle is recorded numerically with a sensitivity of 125 μm $\times$ 125 μm on a photographic plate covered with an X-ray active luminescence surface. The crystallinity χ_c of the samples was estimated by Statton method[7] from the intensity profile of a diffracted X-ray in the range of the scattering angle 2θ from 12° to 32°. We did not use the density column method for the evaluation of crystallinity because the density of amorphous PET varies linearly as a function of amorphous orientation[5] and the crystallinity value cannot be obtained quantitatively for the oriented sample.

Preparation of the Oriented Amorphous Sample

To obtain the molecular-oriented samples without any appreciable crystallization, the slow cold-drawing method in the water was applied to the above original spun yarn. Mitsuishi and Ikeda[8] showed that highly oriented amorphous PET fiber can be obtained by this cold-drawing method. There are two advantages in this cold-drawing method in water: (1) The drawing procedure is carried out almost isothermally even if exothermic necking behavior takes place during the deformation, and (2) in the water, the glass transition temperature is reduced to about 48°C,[9] so

Table I Structural and Mechanical Properties for Oriented Amorphous PET Fibers (Series I)

Water Temp (°C)	$\Delta n \times 10^{-3}$	χ_c (%)	E (GPa)	σ_{break} (GPa)	λ_{break}	σ_{yield} (MPa)	λ_{yield}	λ^0_{net}
Original	1.0	ND	1.56	0.98	10.15	56.2	1.047	1.00
20	162.2	ND	5.58	0.75	2.00	170.9	1.060	4.40
40	139.5	ND	5.82	0.82	2.15	166.9	1.045	4.30
55	111.4	ND	5.03	0.88	2.25	155.3	1.035	4.20
58	95.2	ND	4.44	0.90	2.38	147.9	1.040	4.05
60	75.9	ND	4.03	0.96	2.55	125.1	1.043	3.90
61	66.0	ND	3.74	0.95	2.83	110.3	1.040	3.50
62	54.8	ND	2.98	0.93	2.93	99.8	1.040	3.35
64	37.9	ND	2.66	0.88	3.33	82.7	1.040	2.85
66	11.4	ND	2.24	0.79	4.45	63.1	1.043	2.05
70	3.5	ND	1.88	0.84	6.25	62.5	1.037	1.50

ND: not detected.

that an undesirable generation of crack or craze in the sample during drawing can be avoided as much as possible. In the drawing, the initial length of the original sample was 7 cm and the total elongation ratio was fixed as 4, i.e., the drawn fibers are 28 cm in length. Each sample was drawn with a constant deformation speed of 1.2 mm/min and the temperature of the water was controlled to within an accuracy of ±0.5°C to the predetermined value during the drawing procedure. The temperature of the water was varied from 20 to 70°C so as to obtain samples with a wide range of birefringence Δn. The Δn values of samples obtained by this cold-drawing method are listed in Table I. Hereafter, the oriented amorphous samples thus obtained are denoted as the samples of Series I. The table shows that the drawing at a lower water temperature gives a higher molecular orientation judged from the Δn value and the highest Δn of Series I samples is about $\Delta n = 0.16$ obtained at 20°C.

Annealing Procedure to Obtain the Crystalline Samples

Two series (II and III) of crystallized samples were prepared by annealing, i.e., samples having various degrees of crystallization without orientation and with high orientation, respectively. Annealing was made using a silicone oil bath controlled at given temperatures. Annealing time was fixed as 10 min and the temperature of the silicone oil was varied from 80 to 220°C to obtain the samples with a various range of crystallinity. In the annealing procedure, the sample length was kept constant to prevent shrinkage which causes a significant change in the birefringence value of the sample. The original spun yarns were annealed to prepare the crystallized samples without apparent molecular orientation (Series II). On the other hand, the cold-drawn samples with $\Delta n = 0.16$ obtained at 20°C in water were annealed for the preparation of the crystallized samples with a high molecular orientation (Series III). χ_c and Δn data of samples of Series II and III are shown in Tables II and III, respectively. The tables show that Δn values of the annealed samples are nearly equal to those of the initial unannealed samples employed for Series II and III, respectively.

Tensile Testing

Fiber samples with a 10 mm gauge length were stretched at a constant speed of 1.5 mm/min (which is an initial strain rate of 0.15 min^{-1}) on a constant speed stretching device FGS-50D (Simpo Eng. Co., Japan) at room temperature of ca. 20°C for tensile testing. The load data during elongation were monitored using digital load monitor DFG-0.2KR (Simpo Eng. Co.) and these detected numerical data were directly transferred to a personal computer for recording. The experimental load-extension curves were converted to the stress–strain curves to evaluate the mechanical properties, i.e., initial modulus E, yield stress σ_{yield}, breaking stress σ_{break}, draw ratio at breaking point λ_{break}, and draw ratio at yield point λ_{yield}. In the evaluation of σ_{yield} and σ_{break}, we assumed

Table II Structural and Mechanical Properties for Nonoriented Crystalline PET Fibers (Series II)

Annealing Temp (°C)	$\Delta n \times 10^{-3}$	χ_c (%)	E (GPa)	σ_{break} (GPa)	λ_{break}	σ_{yield} (MPa)	λ_{yield}	λ^0_{net}
No treatment (original)	1.0	ND	1.56	0.98	10.15	56.2	1.047	1.00
105	0.3	6.8	1.44	1.00	11.06	58.3	1.045	0.95
113	0.4	25.4	1.74	0.95	10.60	68.1	1.047	0.97
115	0.4	35.8	1.71	0.83	9.95	70.5	1.050	0.98
119	0.1	45.7	1.94	0.75	8.85	78.9	1.050	1.04
150	0.5	53.8	1.99	0.70	8.76	75.4	1.057	1.01
200	0.8	68.1	1.78	0.41	6.18	77.4	1.050	1.06

ND: not detected.

the incompressibility of the samples to calculate the true stress value.

Measurement of Network Draw Ratio

The concept of a molecular network for the spun yarn which could be regarded as a frozen stretched rubber appears to be reasonable as demonstrated by Ward[1] and Allison and Ward[10] in their investigation on the PET fibers with $\Delta n \leq 9.2 \times 10^{-3}$, showing that the limiting network extensibility ratio $[\lambda_N/(1 - s)]$ is as about 4, irrespective of the initial Δn values of the fiber. Here, λ_N is the natural draw ratio and s is the shrinkage. This result indicates that these spun yarns have intrinsically a unique network structure which does not change during the cold drawing. Brody[11,12] examined a set of stress–strain curves obtained for the cold-drawing spun fibers with a very wide range of initial orientations and found that the thus-obtained stress–strain curves could be superimposed to produce a master stress–strain curve, indicating the existence of an intrinsic network structure which is stretched and frozen through the cold-drawing procedure, and also found that the master curve can be determined as the stress–strain curve for the nonoriented spun yarn. Based on Brody's study, Long and Ward[5] proposed the stress–strain curve matching method for estimating the draw ratio of the network structure (i.e., network draw ratio, λ_{net}) for fiber samples with molecular orientation.

In this work, the initial network draw ratio λ^0_{net} of all fiber samples was evaluated following the curve-matching method by Long and Ward[5]: The load-extension curves for samples were converted into true stress–logarithmic total draw ratio curves assuming a constant volume during elongation. The original yarn was assumed to have no initial drawing of the network structure, i.e., the initial network draw ratio is unity ($\lambda^0_{net} = 1$). The true stress–strain curves of the sample fibers were superimposed on that of the original yarn by the shift of the curve along a strain axis. In the curve-matching procedure, although some arbitration is inevitable, we tried to superimpose the curve in such a manner as to adjust the second-half of the curve to compare the stress–strain curves totally including the breaking phenomenon. It should be noted that, in this method, we

Table III Structural and Mechanical Properties for Oriented Crystalline PET Fibers (Series III)

Annealing Temp (°C)	$\Delta n \times 10^{-3}$	χ_c (%)	E (GPa)	σ_{break} (GPa)	λ_{break}	σ_{yield} (MPa)	λ_{yield}	λ^0_{net}
No treatment	166.4	ND	5.33	1.01	2.33	203.3	1.062	4.40
80	164.1	19.0	5.66	0.70	1.98	182.6	1.055	4.20
110	161.5	25.5	4.97	0.69	1.91	177.4	1.047	4.40
130	162.8	34.4	4.95	0.89	2.20	ND	ND	4.40
150	163.4	45.6	4.63	0.77	1.93	ND	ND	4.80
200	168.4	67.9	4.33	0.80	1.95	ND	ND	4.90

ND: not detected.

need at least one sample whose network draw ratio is known so that the superimposing procedure is available and that is the reason why the original sample yarn was made at a low enough take-up speed to prevent molecular orientation. The initial network draw ratio λ_{net}^0 of a sample is then given as the strain axis shift in the curve matching. The total network draw ratio λ_{net} for a sample during drawing is then given as

$$\lambda_{net} = \lambda_{net}^0 \times \lambda \quad (1)$$

where λ is the imposed (actual) draw ratio in the tensile testing.

RESULTS AND DISCUSSION

Curve Matching and Evaluation of Network Draw Ratio

Figure 1 shows the results of tensile testing for Series I samples. Figure 1(a) shows the true stress data of the oriented amorphous fibers (Series I) plotted as a function of logarithm of actual draw ratio, $\ln(\lambda)$, and in Figure 1(b), these curves have been matched against the stress–strain curve for the original spun yarn by a horizontal shift to give each curve as a function of logarithm of network draw ratio, $\ln(\lambda_{net})$. The initial network draw ratio (λ_{net}^0) of the oriented amorphous samples are evaluated as the shift factor to match against the original spun yarn. As described before, the curve matching was carried out especially so as to adjust the second-half of the curve, therefore, the first-half shows a rather significant deviation from the original spun yarn. Nevertheless, it was confirmed that all the oriented amorphous fibers are able to well superimpose on that of the original spun yarn to give a master curve. This result implies that PET fiber has an intrinsic network structure and the drawing of the fiber corresponds to the stretching of the network, as suggested by Ward,[1] Allison and Ward,[10] and Brody.[11,12]

From the figure, beside λ_{net}^0, other properties (i.e., initial modulus E, the true stress and actual draw ratio at breaking point σ_{break} and λ_{break}, and the true stress and actual draw ratio at yield point σ_{yield} and λ_{yield}) can also be determined, and these are collected in Table I as well as the birefringence Δn and crystallinity χ_c. As described before, the samples of Series I did not show any apparent crystalline X-ray diffraction pattern so that χ_c of these samples were not able to be estimated. The table shows that the Δn values of these amorphous oriented fibers are higher for lower water temperature. As many researchers have pointed out,[1–4] Δn has a strong correlation with the mechanical properties of the fiber and the table shows that E and σ_{yield} are higher for higher Δn, whereas λ_{break} is lower for higher Δn. As can be expected, the value of λ_{net}^0 increases as Δn increases and this result is consistent with Long

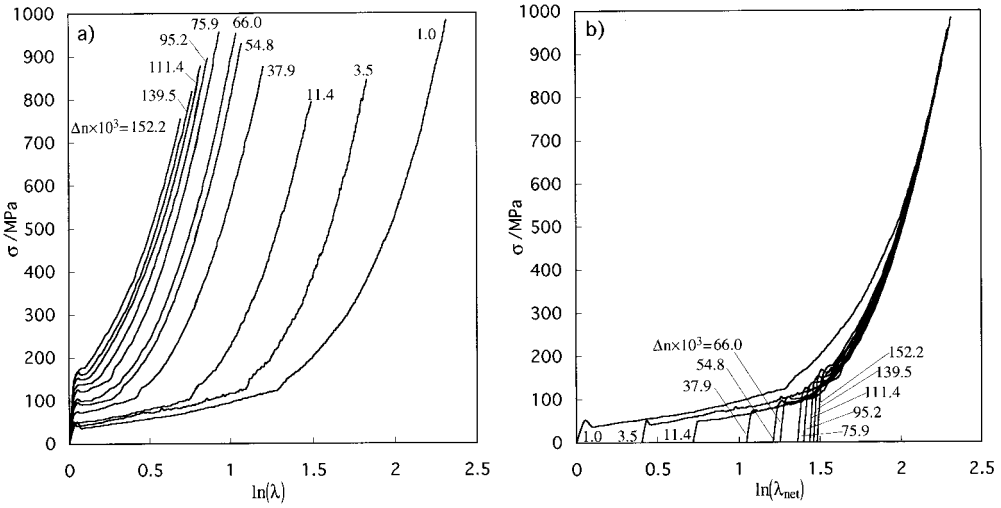

Figure 1 True stress–strain curves for oriented amorphous samples (Series I): (a) true stress vs. logarithm of imposed (actual) draw ratio [$\ln(\lambda)$]; (b) true stress vs. logarithm of network draw ratio [$\ln(\lambda_{net})$]. Shift factors are determined by matching of true stress–strain curves for the original spun yarn.

and Ward.[5] Table I also shows that σ_{break} and λ_{yield} are not significantly affected by the Δn value of the fibers for Series I.

Although the curve-matching method carried out here is the same, in principle, as that of Long and Ward,[5] the superimposing nature is relatively better in Figure 1(b), especially in the low λ_{net} region. This is presumably due to the fact that samples without apparent crystallinity were subjected in Figure 1(b), differing from their work in which practically crystallized fibers were used. The effects of crystallinity on the curve matching will be discussed later.

Figure 2 shows similar plots for the nonoriented crystallized samples (Series II) as in Figure 1, and the results are listed in Table II. All the samples of Series II have a molecular orientation less than that of original spun yarn, although the values of χ_c varies from practically 0 up to 68.1%, corresponding to the annealing temperature. In contrast to Series I, all the true stress–strain curves are rather similar with the original spun yarn, leading to a small amount of shift to obtain the master curve—hence, nearly equal values of λ_{net}^0 ($\approx$ 1.0). This suggests that for the nonoriented samples the true stress–strain curves are not significantly affected by the crystallinity and that the existence of crystalline phase does not practically affect the intrinsic network structure of the original spun yarn.

In spite of good matching shown in Figures 1(b) and 2(b), a significant deviation from the master curve is rather noticeable in the low λ_{net} region [ca. $\ln(\lambda_{net}) < 1.5$] for each curve and this region practically corresponds to the neck drawing region. It should be noted that the manner of deviation is different in Figures 1(b) and 2(b), i.e., in the former, a true stress–strain curve appears in the lower stress side of the master curve and the deviation is higher for the higher Δn sample; on the other hand, in the latter, the reverse is true and the deviation is higher for the higher χ_c sample. It means that the drawing stress is lower for the higher oriented sample and is higher for the higher crystallinity sample, i.e., alignment of polymer chains by necking becomes easier for oriented samples and harder for crystallized samples.

Figure 3 and Table III are for the oriented crystallized samples (Series III). As shown in Figure 3(a), the true stress–strain curves for the samples of Series III are completely different from that of the original yarn and the highly crystallized samples with $\chi_c > 45\%$ do not show the yield point, resulting in the different shape of the curve from that of low crystallinity samples. Nevertheless, the curve-matching method proved excellent, as shown Figure 3(b). Table III also shows that the E values are lower and λ_{net}^0 values are higher for samples with $\chi_c > 45\%$. Note that λ_{net}^0 for the lower crystallinity samples with $\chi_c < 45\%$ is almost the same as that of the unannealed sample having practically no crystallinity. This suggests that the intrinsic network structure can also be

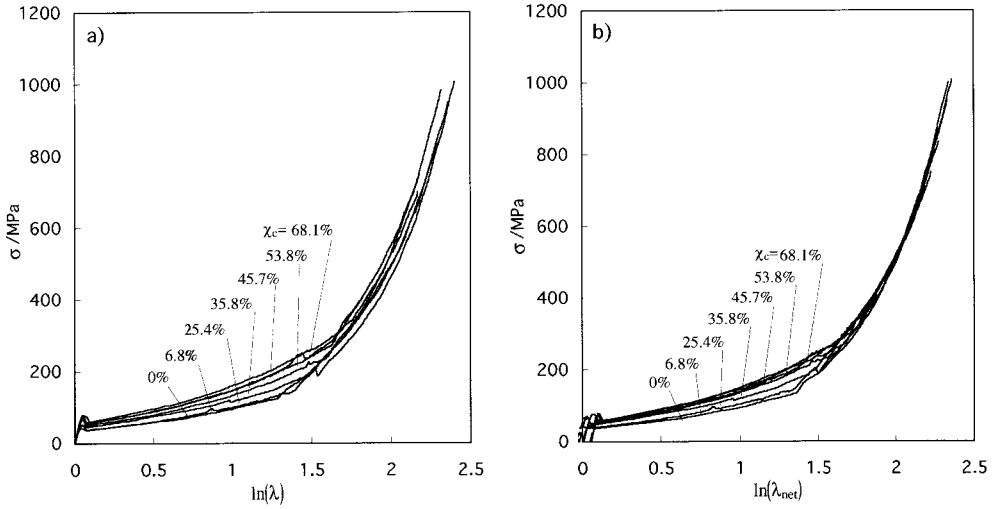

Figure 2 True stress–strain curves for nonoriented crystalline samples (Series II): (a) true stress vs. logarithm of imposed (actual) draw ratio [$\ln(\lambda)$]; (b) true stress vs. logarithm of network draw ratio [$\ln(\lambda_{net})$]. Shift factors are determined by matching of true stress–strain curves for the original spun yarn.

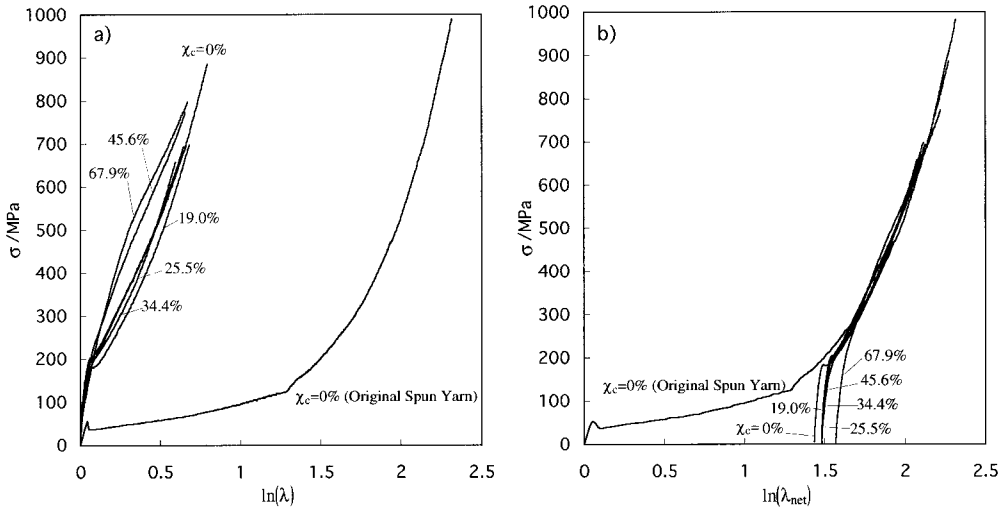

Figure 3 True stress–strain curves for oriented crystalline samples (Series III): (a) true stress vs. logarithm of imposed (actual) draw ratio [ln(λ)]; (b) true stress vs. logarithm of network draw ratio [ln(λ_{net})]. Shift factors are determined by matching of true stress–strain curves for the original spun yarn.

well preserved for the oriented crystalline samples with $\chi_c < 45\%$. For the oriented crystalline samples with $\chi_c > 45\%$, the network structure is changed to some extent judged from λ^0_{net}, making the tensile properties slightly deviated from those for the lower crystalline samples.

Figure 4 shows the relationship between birefringence Δn and λ^0_{net} for all the samples. λ^0_{net} values of Series I samples show a wide variation due to the wide variation of Δn. It is confirmed that λ^0_{net} increases with an increase in Δn as Long and Ward[5] reported for drawn and heat-set yarns. λ^0_{net} values for Series II are almost unity, irrespective of crystallinity, which seems to be quite reasonable because the original Δn value before annealing is expected to be kept almost the same due to the constant length treatment. For Series III samples, λ^0_{net} values largely deviate—nevertheless, the almost constant Δn. Seeing the $\Delta n - \lambda^0_{net}$ relation on the whole, only two samples in Series III seem to deviate from the relation. These two samples are characterized by higher χ_c (>45%) and no yield point appearance in the stress–strain curve. It can be considered that the intrinsic network structure for highly oriented samples might be extended by the strong shrinkage tension caused by the crystallization over some threshold value (here, about $\chi_c = 45\%$).

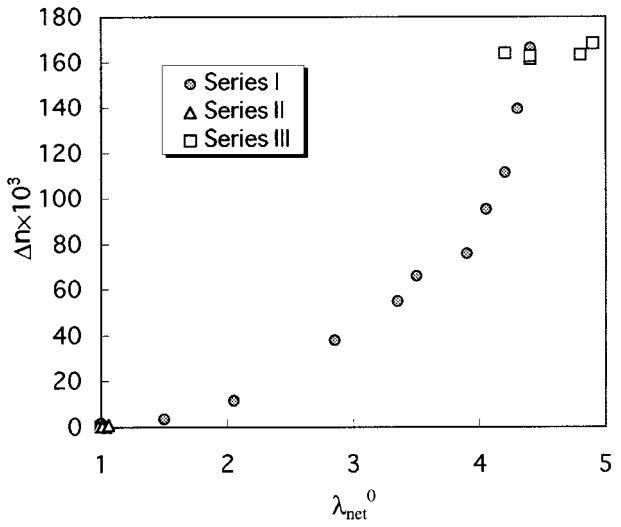

Figure 4 Relationship between birefringence Δn and initial network draw ratio λ^0_{net} for all the sample.

It should be noted that Δn and λ^0_{net} do not have a monotonous correlation even for Series I and Δn increases significantly in the region of about before $\lambda^0_{net} = 4.0$. Shirataki et al.[13] investigated an increase in Δn for cold-drawn PET fibers in terms of the network draw ratio concept and they suggested that the transition of the deformation mechanism is caused in the cold-drawing procedure for preparing the sample with $\lambda_{net} > 3.7$, i.e., affine deformation in lower λ_{net} region changes to a pseudoaffine deformation in the higher λ_{net} region. It is, therefore, appropriate to regard that the significant increases in Δn around $\lambda_{net} = 4.0$ shown in Figure 4 corresponds to the transition of the deformation mechanism.

Correlation Between Initial Modulus and Network Draw Ratio

As Tables I–III show, the initial modulus E of the samples tends to be higher for higher λ_{net}^0 samples. Long and Ward[5] showed that the variation of the modulus of hot-drawn PET fibers are well plotted as a function of network draw ratio irrespective of the difference in the drawing procedure.

Figure 5 shows the variation of measured initial modulus E vs. λ_{net}^0 [Fig. 5(a)] and vs. Δn [Fig. 5(b)] for all samples. In Figure 5(a), the modulus shows good correlation with λ_{net}^0 in a similar manner with the results of Long and Ward.[5] This suggests the possibility that E of those PET fibers can be expressed as a function of λ_{net}^0 quantitatively. According to this point of view, the aggregate model proposed by Ward[14–16] is applied to obtain the modulus value theoretically. On the other hand, we also tried to apply the rubber network model with some modification for the same purpose as described later.

The aggregate[14–16] model seems to be the most promising method to relate E to λ_{net}^0. In this model, a partially oriented fiber is assumed to consist of an aggregate of anisotropic units and each unit has transverse isotropy making a certain angle with the fiber axis. The modulus of the fiber can be evaluated from two different averaging procedures for an aggregate units which are arranged within the fiber according to the degree of orientation, i.e., one is averaging the compliance constants and the other is averaging the stiffness constants. The averaging of the compliance and stiffness constants are called the Reuss average and the Voigt average, respectively. These procedures give the lower and upper bounds for the elastic constants and the aggregate model predicts that the elastic constants should lie between the Reuss and Voigt average values (E_R and E_V).

Comparisons of the predicted extensional moduli of fibers by the aggregate model with those measured in the experimental study were given by Allison and Ward[10] and Hadley et al.,[17] and for PET fiber, it has been shown that the measured values lie close to the mean values of E_R and E_V.

The compliance averaging procedure (Reuss average) gives the extensional modulus E, denoted by E_R, which is[10]

$$\frac{1}{E_R} = \overline{s_{33}} = I_1 s_{11} + I_2 s_{33} + I_3(2s_{13} + s_{44}) \quad (2)$$

where s_{11}, s_{13}, s_{33}, and s_{44} are the compliances for a fully oriented fiber and I_1, I_2, and I_3 are the orientation parameters for the partially oriented fiber.

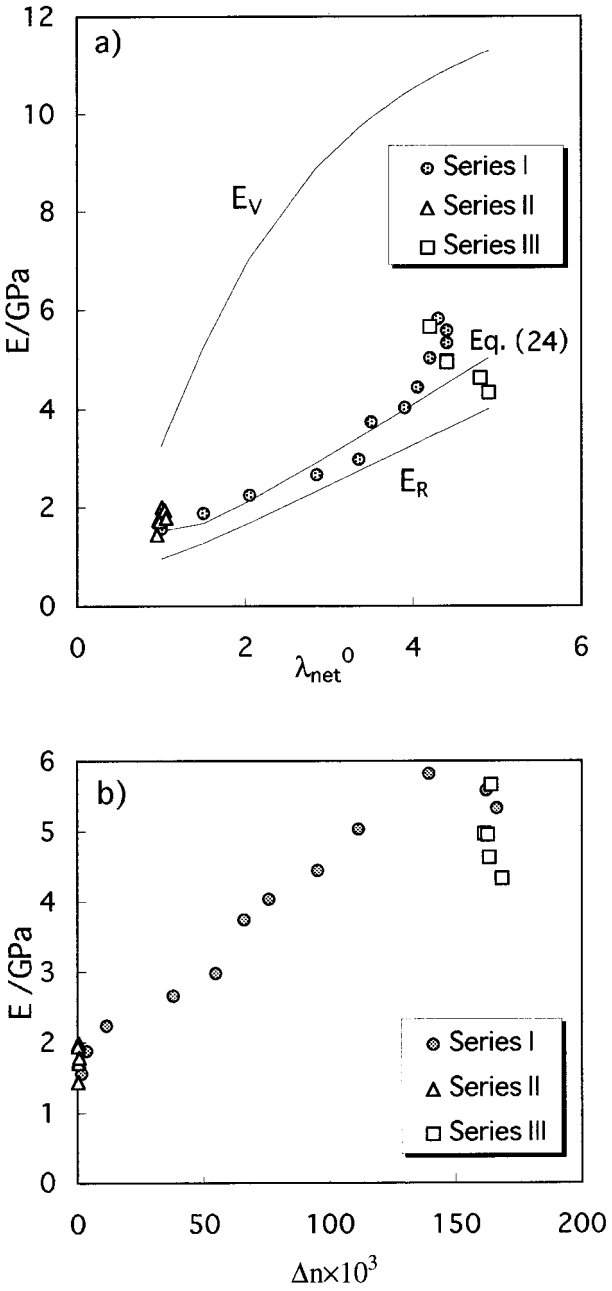

Figure 5 Initial modulus E vs. (a) initial network draw ratio λ_{net}^0 and (b) birefringence Δn. Calculated lines by the aggregate model (E_R and E_V) and that by using eq. (24) are denoted in (a).

The measured values of s_{11}, s_{13}, etc., for a highly oriented PET fiber ($\Delta n = 0.187$) which were given by Allison and Ward[10] are shown in Table IV. The orientation parameters are expressed as a function of draw ratio as[15]

Table IV Compliance Constants ($\times 10^{-11}$ m²/N) for Highly Oriented PET with $\Delta n = 0.187$

S_{11}	s_{13}	s_{33}	s_{44}	s_{12}
160	−3.1	7.1	140	−58

Given by Allison and Ward.[10]

$$I_1 = \frac{K^4}{(1-K^2)^2}\left\{1 + \frac{1}{2K^2} + \frac{(\frac{1}{2} - 2K^2)\cos^{-1}K}{K^3(1-K^2)^{1/2}}\right\} \quad (3)$$

$$I_2 = \frac{1}{(1-K^2)^2}\left\{1 + \frac{K^2}{2} - \frac{3K\cos^{-1}K}{2(1-K^2)^{1/2}}\right\} \quad (4)$$

$$I_3 = \frac{K^2}{(1-K^2)^2}\left\{-\frac{3}{2} + \frac{(1+2K^2)\cos^{-1}K}{2K(1-K^2)^{1/2}}\right\} \quad (5)$$

$$I_4 = \frac{K^2}{1-K^2}\left\{-1 + \frac{\cos^{-1}K}{K(1-K^2)^{1/2}}\right\} \quad (6)$$

$$I_5 = \frac{1}{1-K^2}\left\{1 - \frac{K\cos^{-1}K}{(1-K^2)^{1/2}}\right\} \quad (7)$$

where $K = \lambda^{-3/2}$. Here, orientation parameters I_4 and I_5 are also denoted although these are not used in eq. (2) because they are necessary to calculate the Voigt average modulus E_V later.

It is appropriate to use λ^0_{net} instead of λ in the formula of $K = \lambda^{-3/2}$, because λ^0_{net} is the exact evaluation for the draw ratio of the network structure. Thus, the modulus of the PET fiber with a known λ^0_{net} can be calculated based on the Reuss average procedure described above and that is denoted as E_R. The results are shown in Figure 5(a).

The aggregate model provides the other procedure to give the modulus value. The stiffness averaging procedure which is called the Voigt average also gives E, denoted by E_V. The value of E_V is calculated as $1/\overline{s'_{33}}$, where $\overline{s'_{33}}$ is obtained by inverting the matrix of the stiffness constant for the partially oriented fiber ($\overline{c'_{11}}$, $\overline{c'_{12}}$, etc.) and is given by

$$\overline{s'_{33}} = \frac{\overline{c'_{12}}(\overline{c'_{12}} + \overline{c'_{11}})}{\overline{c'_{33}c'_{12}}(\overline{c'_{12}} + \overline{c'_{11}}) - 2\overline{c'_{12}c'_{13}}^2} \quad (8)$$

where $\overline{c'_{11}}$, $\overline{c'_{12}}$, etc., are given by averaging over an aggregate of anisotropic units as follows:

$$\overline{c'_{11}} = \overline{c'_{22}} = \tfrac{1}{8}(3I_2 + 2I_5 + 3)c_{11} + \tfrac{1}{4}(3I_3 + I_4)c_{13} + \tfrac{3}{8}I_1c_{33} + \tfrac{1}{2}(3I_3 + I_4)c_{44} \quad (9)$$

$$\overline{c'_{12}} = \tfrac{1}{8}(I_2 - 2I_5 + 1)c_{11} + I_5c_{12} + \tfrac{1}{4}(I_3 + 3I_4)c_{13} + \tfrac{1}{8}I_1c_{33} + \tfrac{1}{2}(I_3 - I_4)c_{44} \quad (10)$$

$$\overline{c'_{13}} = \tfrac{1}{2}I_3c_{11} + \tfrac{1}{2}I_4c_{12} + \tfrac{1}{2}(I_1 + I_2 + I_5)c_{13} + \tfrac{1}{2}I_3c_{33} - 2I_3c_{44} \quad (11)$$

$$\overline{c'_{33}} = I_1c_{11} + I_2c_{33} + 2I_3(c_{13} + 2c_{44}) \quad (12)$$

$$\overline{c'_{44}} = \tfrac{1}{4}(2I_3 + I_4)c_{11} - \tfrac{1}{4}I_4c_{12} - I_3c_{13} + \tfrac{1}{2}I_3c_{33} + \tfrac{1}{2}(I_1 + I_2 - 2I_3 + I_5)c_{44} \quad (13)$$

where c_{11}, c_{12}, $\cdots$ are the stiffness constants of a fully oriented fiber which have not been determined experimentally. These constants, however, can be obtained by an inverting compliance matrix[14] and expressed as a function of compliance components as

$$c_{11} = \frac{s_{12}(s_{11}s_{33} - s_{13}^2)}{(s_{12} - s_{11})\{2s_{13}^2s_{12} - s_{33}s_{12}(s_{12} + s_{11})\}} \quad (14)$$

$$c_{12} = \frac{s_{12}(s_{13}^2 - s_{33}s_{12})}{(s_{12} - s_{11})\{2s_{13}^2s_{12} - s_{33}s_{12}(s_{12} + s_{11})\}} \quad (15)$$

$$c_{13} = \frac{s_{12}s_{13}}{2s_{12}s_{13}^2 - s_{33}s_{12}(s_{12} + s_{11})} \quad (16)$$

$$c_{33} = \frac{s_{12}(s_{12} + s_{11})}{s_{33}s_{12}(s_{12} + s_{11}) - 2s_{12}s_{13}^2} \quad (17)$$

$$c_{44} = \frac{1}{s_{44}} \quad (18)$$

Calculated E_V values are also shown in Figure 5(a) with E_R, and as shown in the figure, E_V is always higher than is E_R.

The aggregate model predicts that the measured modulus values lie between the values of E_R and E_V. Figure 5(a) confirms this prediction and the measured values are exactly plotted in the region between E_R and E_V. However, Figure 5(a) indicates that, in this evaluation, measured values lie much closer to E_R than to E_V. This result differs from that by Allison and Ward[10] and it may be caused by the difference of the draw ratio in the orientation parameters [eqs. (3)–(7)]. In this study, λ^0_{net} is used as draw ratio in

$K = \lambda^{-3/2}$ for the orientation parameters, whereas in the study of Allison and Ward, the natural draw ratio, which is determined as the ratio of the cross-sectional area before and after stretching, was used for the same purpose. It means that the Reuss average gives a good approximation for the initial modulus in the case when λ_{net}^0 is used as the draw ratio for orientation parameters. It should be noted that the aggregate model gives a good estimation for the modulus nonempirically if the compliance for a fully oriented fiber is known.

In this study, we also attempted another procedure to give a modulus as a function of the network draw ratio by using rubber network model with some modification. Principally, E is defined as a gradient of stress at draw ratio $\lambda = 1$ as follows:

$$E = \left.\frac{\partial \sigma}{\partial \lambda}\right|_{\lambda=1} = \left.\frac{\partial F}{\partial \lambda}\right|_{\lambda=1} = \left.\frac{\partial^2 U}{\partial \lambda^2}\right|_{\lambda=1} \quad (19)$$

where σ is stress; F, the force per unit cross-sectional area of the undeformed sample, and U, the strain-energy function corresponding to the Helmholtz free energy of the strain. From the classical rubberlike elasticity model, U for uniaxial deformation under the incompressibility condition is expressed as[14]

$$U = \frac{1}{2} NkT\left(\lambda^2 + \frac{2}{\lambda} - 3\right) \quad (20)$$

where N is the number of chains per unit volume in the network (i.e., network density); k, the Boltzmann constant, and T, Kelvin temperature. By substituting eq. (20) into eq. (19), E is given as

$$E = NkT\left(1 + \frac{2}{\lambda^3}\right)\Bigg|_{\lambda=1} = 3NkT \quad (21)$$

Equation (21) gives the correlation between initial modulus and network density. It should be noted that eq. (21), however, is only applicable for the initial deformation of the sample without any initial network extension. It follows that for practical expression of the initial modulus the effect of the previous network extension, i.e., the initial network draw ratio, should be taken into account in eq. (19) and this is realized by a quite simple procedure.

When the network is strained up to $\lambda = \lambda_{net}^0$, the stress is given as

$$\sigma = \lambda \left.\frac{\partial U}{\partial \lambda}\right|_{\lambda=\lambda_{net}^0} \quad (22)$$

Then, the modulus at a draw ratio of λ_{net}^0 is given as a gradient of the stress at $\lambda = \lambda_{net}^0$ as follows:

$$E = \left.\frac{\partial \sigma}{\partial \lambda}\right|_{\lambda=\lambda_{net}^0} = \left.\frac{\partial}{\partial \lambda}\left(\lambda \frac{\partial U}{\partial \lambda}\right)\right|_{\lambda=\lambda_{net}^0}$$

$$= \left.\left(\frac{\partial U}{\partial \lambda} + \lambda \frac{\partial^2 U}{\partial \lambda^2}\right)\right|_{\lambda=\lambda_{net}^0} \quad (23)$$

Substituting eq. (20) into eq. (23) gives the initial modulus of extended network under the condition of a classical rubberlike elasticity model as eq. (24):

$$E = NkT\left[\left(\lambda - \frac{1}{\lambda^2}\right) + \lambda\left(1 + \frac{2}{\lambda^3}\right)\right]\Bigg|_{\lambda=\lambda_{net}^0} \quad (24)$$

This equation indicates that the initial modulus is variable with a network extension even for the constant network density and eq. (24) gives an E value for the sample with an arbitrary nonunity λ_{net}^0. In the case of $\lambda_{net}^0 = 1$ (i.e., no initial network extension), eq. (24) exactly reduces to eq. (21). The value of NkT can be evaluated from the experimental result of E for the original yarn with $\lambda_{net}^0 = 1$ in eq. (24) [or in eq. (21)] as $NkT = 5.20 \times 10^8$ (or $N = 1.28 \times 10^{29}$ m^{-3} for $T = 20$°C). Then, the E values of nonunity λ_{net}^0 samples of this network structure can be estimated using eq. (24).

As shown in Figure 5(a), E for Series I samples increases with increase in λ_{net}^0. Experimental E values for Series I show good agreement with those calculated using eq. (24) up to about $\lambda_{net}^0 = 4.0$, then deviate from the theory, followed by an abrupt increase in the region of $\lambda_{net}^0 > 4.0$. Thus, the validity of eq. (24) is noticeable up to $\lambda_{net}^0 = 4.0$, which corresponds to the point of transition of deformation mechanism shown in Figure 4. On the one hand, $\lambda_{net}^0 = 4.0$ shown above exactly corresponds to the natural draw ratio for cold drawing of the amorphous PET fiber with $\Delta n \approx 1.0 \times 10^{-3}$ (Refs. 9 and 10) and this value can also be regarded as the limit of the natural extension of the network structure for PET fibers as described before.[10] It is considered that the transi-

tion of the deformation mechanism from affine deformation (rubber deformation) to pseudoaffine deformation at $\lambda_{net}^0 \approx 4.0$ is caused by significant increases in the drawing stress during the cold drawing in water due to the strain-hardening effect,[11,18,19] which cannot be taken into account in classical rubber model that we used in eq. (24).

The alternative way is to use a theory with the potential for the strain-hardening effect such as the theory of Ball et al.[20] or Edwards and Vilgis,[21] and substitute the free energy given by those theories into eq. (23). In this article, we do not attempt to use those sophisticated theories because they include several unknown parameters which should be adjusted by the fitting method and too many unknown parameters make the situation complicated.

Figure 5(a) also shows that the measured results for Series II and III seem not to follow the same tendency as that of Series I, i.e., the E values of Series III decrease with increase in λ_{net}^0 and the E value of Series II rather scatters at almost same λ_{net}^0. This is obviously caused by the effect of crystallinity and, unfortunately, we do not have a sufficient quantitative explanation to clarify the relationship between mechanical properties and crystallinity.[3] Conclusively, even with all those deviations caused by strain hardening and crystallinity, the model based on the concept of the network draw ratio provides a good estimation for the initial modulus as shown in Figure 5(a).

Figure 5(b) indicates that the initial modulus E increases as birefringence Δn increases; however, for the samples with $\Delta n > 0.16$ and samples with $\Delta n \approx 1.0 \times 10^{-3}$ (nonoriented), E values exhibit a significant decreasing feature and scattering feature, respectively. These features are much the same as observed for the $E - \lambda_{net}^0$ relation.

Correlation Between Yield Stress and Network Draw Ratio

Tables I–III indicate that the yield stress σ_{yield} tends to increase with increase in λ_{net}^0 in a similar manner with an initial modulus E, suggesting that σ_{yield} also has a quantitative correlation with the network draw ratio. The superimposed curves shown in Figures 1(b), 2(b), and 3(b) suggest that the true stress–strain curve of the original nonoriented amorphous yarn can be approximately taken as the master curve for the intrinsic network structure. From this point of view, the yield points for nonunity λ_{net}^0 samples themselves might fall on the master curve (true stress – λ_{net}^0 curve) if the σ_{yield} is plotted against λ_{net}^0.

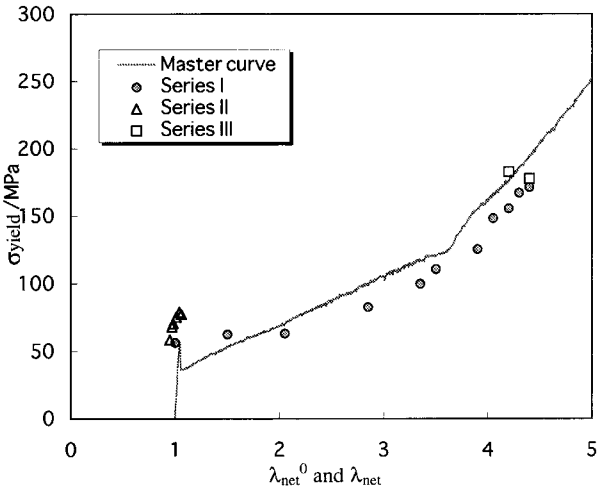

Figure 6 Relationship between yield stress σ_{yield} and initial network draw ratio λ_{net}^0. The true stress–strain curve for the original spun yarn (master curve) is denoted for comparison.

The validity of the above assumption is clearly pictured in Figure 6, where the variation of σ_{yield} vs. λ_{net}^0 for all the samples is shown and the master curve is indicated in the figure as well. As shown in the figure, the σ_{yield} value of the sample with given λ_{net}^0 are well evaluated as the true stress value on the master curve at λ_{net} which corresponds to λ_{net}^0. This is effective not only for amorphous samples but also for crystallized samples, indicating the reliability of the model of the PET fiber with the intrinsic network structure and that yield stress of an arbitrary sample is determined by the extension of the network structure, i.e., λ_{net}^0.

Correlation Between Breaking Properties and Network Draw Ratio

The idea of the intrinsic network structure implies the existence of the limiting draw ratio of the sample during tensile testing, i.e., samples would break at the certain network draw ratio irrespective of the initial molecular orientation. In Figure 7(a), the values of the imposed draw ratio in the tensile testing at breaking point λ_{break} are plotted as a function of Δn for Series I samples. Figure 7(b) shows the relation between network draw ratio at the breaking point $\lambda_{net,break}$ and Δn, where $\lambda_{net,break}$ is defined as follows:

$$\lambda_{net,break} = \lambda_{net}^0 \times \lambda_{break} \quad (25)$$

Figure 7(a) shows that the λ_{break} varies from as high as 10 for original yarn to as small as 2 for the high oriented sample with $\Delta n \approx 0.16$. On the other hand, $\lambda_{net,break}$ varies between 10 and 8.5 for all the Series I samples, irrespective of Δn. It indicates that the breaking takes place at relatively narrow range of network draw ratio, irrespective of the λ^0_{net} value.

In a similar way, λ_{break} and $\lambda_{net,break}$ for samples of Series II ($\Delta n \approx 0.001$) and III ($\Delta n \approx 0.16$) are plotted against crystallinity χ_c in Figure 8(a) and (b), respectively. The χ_c dependence of λ_{break} for both series of samples are completely different each other: λ_{break} of Series II samples clearly depends on χ_c, decreasing from about 10 to 6 as χ_c increases and λ_{break} for Series III samples is not very much dependent on χ_c, being around 2, irrespective of χ_c. On the other hand, the $\lambda_{net,break}$ values for Series II and III samples plotted in Figure 8(b) almost all fall in the range of between 8 and 10, irrespective of χ_c, although $\lambda_{net,break}$ for the Series II samples shows a slight decreasing function of χ_c.

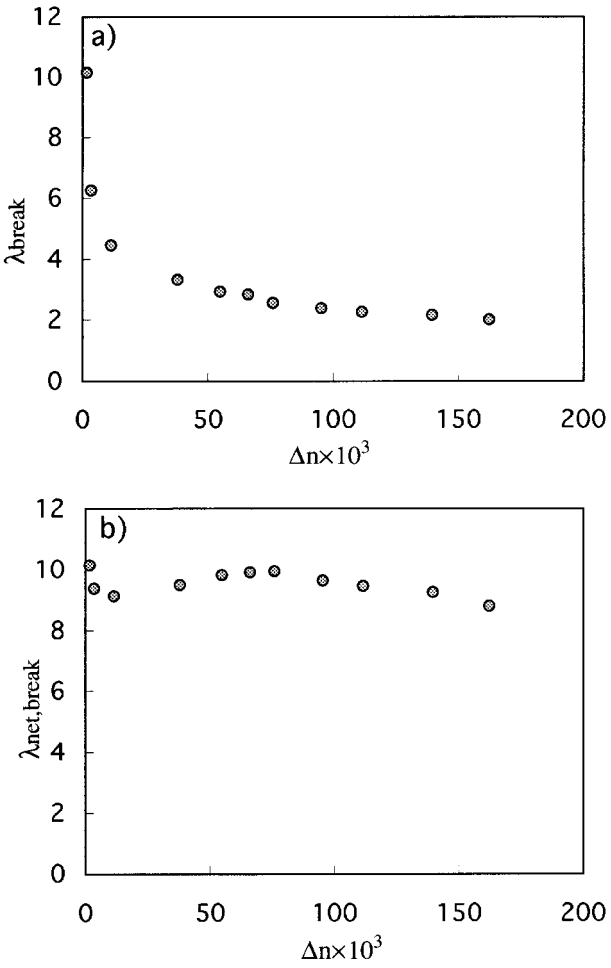

Figure 7 Relationship between draw ratios at breaking point (λ_{break} and $\lambda_{net,break}$) and birefringence Δn for Series I samples: (a) imposed draw ratio at breaking point λ_{break} vs. Δn; (b) network draw ratio at breaking point $\lambda_{net,break}$ vs. Δn.

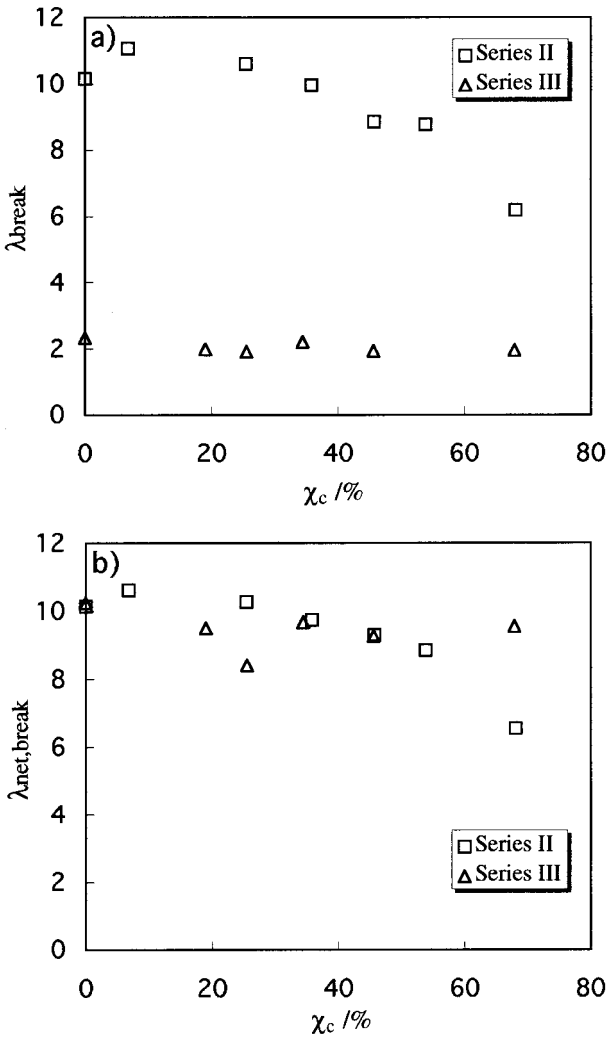

Figure 8 Relationship between draw ratio at breaking point (λ_{break} and $\lambda_{net,break}$) and crystallinity χ_c for Series II and III samples: (a) imposed draw ratio at breaking point λ_{break} vs. Δn; (b) network draw ratio at breaking point $\lambda_{net,break}$ vs. Δn.

The inspection of Figures 7 and 8 suggests that in the tensile test breaking of the fibers would take place at about $8 < \lambda_{net,break} < 10$, irrespective of initial molecular orientation or crystallinity. In other words, $\lambda_{net,break} \approx 10$ can practically be considered as the limiting extension ratio of the intrinsic network structure, where the network structure breaks. The limiting extension ratio of

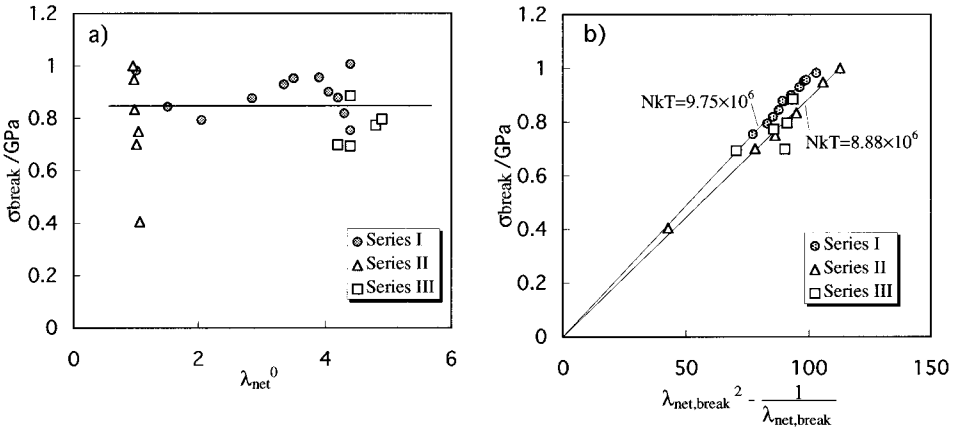

Figure 9 Relationship between true stress at breaking point σ_{break} and initial network draw ratio λ^0_{net}.

the network λ_{limit} is able to be theoretically estimated as a ratio of the diameter of a coiled polymer of a Gaussian chain to a polymer chain length, and that is

$$\lambda_{limit} \approx \frac{bN_p}{bN_p^{1/2}} = N_p^{1/2} \tag{26}$$

where b is monomer length and N_p is degree of polymerization.

The number-average degree of polymerization of the original polymer used in this study is about 109 (=21,000/192; 192 is molecular weight of monomer unit) and it follows that the theoretical limiting extension ratio for breaking is approximately evaluated as $\lambda_{limit} \approx 10$. This theoretical value is surprisingly consistent with the $\lambda_{net,break}$ value which has been evaluated experimentally as described before.

This result also suggests that the network draw ratio at the breaking point depends on the degree of polymerization (i.e., molecular weight of the polymer) as in the manner of $\lambda_{net,break} \approx N_p^{1/2}$ and this expectation seems to be reasonable empirically. It also suggests that the network structure itself is dependent on the molecular weight and other mechanical properties besides those at the breaking point, such as initial modulus and yield stress, are also varied with the molecular weight as well.

Figure 9(a) shows the relationship between true breaking stress σ_{break} and λ^0_{net} for all samples. Although σ_{break} values seem to be rather scattered, almost all of data points are sited in the region of 0.8 ± 0.2 GPa and this scale of deviation (±25%) is significantly small compared with the deviation of actual draw ratio at breaking point (λ_{break} = 6.5 ± 4.5, i.e., almost ±70%). The discussion given before on Figures 7 and 8 makes it noticed that a relatively small deviation of σ_{break} can be explained by the limiting extension ratio of the network structure at the breaking point. If the breaking of the intrinsic network structure takes place at a constant network draw ratio, it follows that the true breaking stress should be constant as well. From the results shown in Figures 7 and 8, for all the samples, the network draw ratio at the breaking point is in the range of $\lambda_{net,break}$ = 9.0 ± 1.0 (deviation ± 10%) and it is appropriate to regard that this small deviation of the $\lambda_{net,break}$ value results in the small deviation of σ_{break} as well. In consequence, all these considerations are based on the model of a unique network structure, therefore suggesting that the small deviation of true breaking stress can only be explained by assuming the intrinsic network structure which is roughly independent of crystallinity and governs the mechanical properties during the tensile testing.

For the classical rubber model, true stress σ is correlated with draw ratio λ under the incompressibility condition as[14]

$$\sigma = \lambda \frac{\partial U}{\partial \lambda} = NkT\left(\lambda^2 - \frac{1}{\lambda}\right) \tag{27}$$

Equation (27) indicates that σ is proportional to $\lambda^2 - 1/\lambda$ with a slope of NkT. In Figure 9(b), σ_{break} values are plotted as a function of $\lambda^2_{net,break} - 1/\lambda_{net,break}$. This figure shows that σ_{break} values satisfies eq. (27) with respect to $\lambda_{net,break}$, i.e., the

network density is constant for each series of samples at the breaking point, although data points are rather scattered for Series II and III. From the slope of each line, $NkT = 9.75 \times 10^6$ ($N = 2.41 \times 10^{27}$ m^{-3} for $T = 20$°C) for Series I samples and $NkT = 8.88 \times 10^6$ ($N = 2.195 \times 10^{27}$ m^{-3} for $T = 20$°C) for Series II and III samples are given, respectively. This means that the crystallinity slightly affects the decrease of the network density of the sample. It also should be noted that these values of network density are much smaller than that obtained from initial modulus ($N = 1.28 \times 10^{29}$ m^{-3}). These suggest that the network density might change greatly during the elongation and that the classical rubber model is not sufficient enough to describe the network structure of PET fiber for a wide range of the extension ratio.

To clarify this problem of the network density, the true stress values σ during the tensile testing are plotted as a function of $\lambda_{net}^2 - 1/\lambda_{net}$ in Figure 10. This figure shows another type of true stress–strain curve based on eq. (27) for samples of Series I–III in Figure 10(a)–(c), respectively. All curves show an abrupt jump of the σ value at the beginning of the deformation which corresponds to the yield behavior, followed by rather linear increase along the axis of $\lambda_{net}^2 - 1/\lambda_{net}$. Although Series I samples among the samples show some deviation in the lower λ_{net} region, the figure indicates that eq. (27) is generally applicable after the yield point and a constant NkT value can be determined as a slope of the line for all series of samples, suggesting that almost a unique network density could be considered for all samples. It follows that PET fiber behaves as an ideal rubber during the tensile testing after the yield point, irrespective of crystallinity and molecular orientation.

The true stress–strain curve of the original spun yarn, i.e., the master curve in the figure, gives a slope of $NkT = 9.75 \times 10^6$ ($N = 2.41 \times 10^{27}$ m^{-3}). This is the same value as that evaluated for Series I samples from the breaking behavior. Figure 10(b) and (c) indicates that the breaking points for crystallized samples tend to be lower than the master curve. This deviation can be caused by a structural defect such as crack or craze generated in the crystallization procedure and the lower NkT value for Series II and III in Figure 9(b) is reasonably explained by this slight decrease of the breaking stress, i.e., an intrinsic network density is also applicable for the samples of Series II and III.

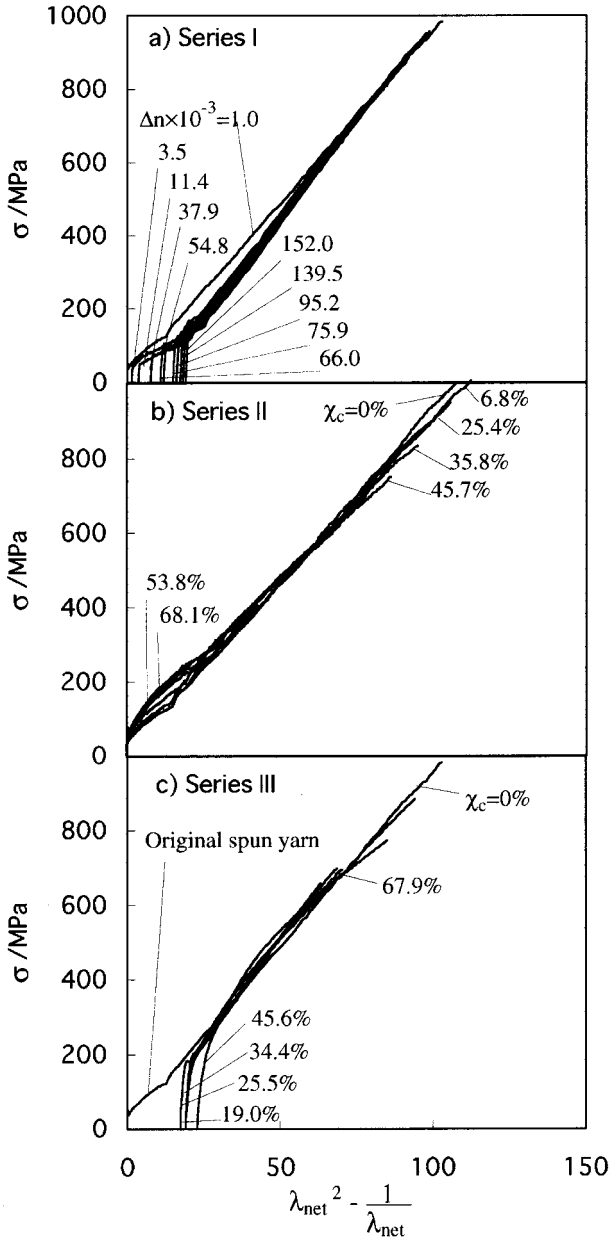

Figure 10 True stress–strain curves plotted according to eq. (27) using network draw ratio: (a) Series I; (b) Series II; (c) Series III.

In this regard, Rietsch et al.[22] evaluated the N value for PET film as 1.89×10^{26} m^{-3}, which is significantly lower than our N value, from the relationship between Δn and $\lambda^2 - 1/\lambda$ for the drawn samples at 80°C in the air, extending in the range of $1.02 < \lambda < 4.6$ under the homogeneous strain for drawing. In contrast, in this article, the N value was estimated by cold drawing (at 20°C) in which samples are extended up to $\lambda \approx 10$, so we cannot simply compare our N value with Rietsch

et al.'s value. The dependence of the network density on temperature and deformation rate has been indicated experimentally for PET fiber.[23]

The network density of the original yarn at the beginning of the deformation evaluated from initial modulus is, however, two digits larger than that determined from the master curve in Figure 10. The reasonable model to explain this network density seems that the network structure is completely different before and after the yield point. It means that the other network structure governs the initial tensile properties and the yield point is regarded as a connecting point between two different network structures. In this article, we cannot describe in detail the structural and physical differences in these two network structures. What is certain is that the initial network structure is also extended by the cold drawing in water and that the strain-hardening effect should be considered as described in Figure 5.

Finally, Figure 10 indicates that if the sample has an unique network structure, by taking into account the network draw ratio, the true stress–strain curve of the sample can be superimposed to a linear line which passes the origin of the coordinate axes of the figure. It means that the plot of true stress σ vs. $\lambda_{net}^2 - 1/\lambda_{net}$ provides a new method to evaluate the network draw ratio. In this method, the λ_{net}^0 value is determined so that the σ vs. $\lambda_{net}^2 - 1/\lambda_{net}$ curve is matched to the linear line passing the origin of the coordinate axes. This method is especially recommended in the case when the sample with a predetermined λ_{net}^0 value cannot be prepared.

CONCLUSION

The relationships between the mechanical properties and network draw ratio have been investigated for PET fibers with different molecular orientation and crystallinity. The matching procedure of true stress–strain curves revealed that PET fiber has a unique intrinsic network structure which is characterized by the network draw ratio. The investigation of tensile properties for the samples in terms of the network draw ratio have shown that (1) practically, crystallization does not affect the network structure, and (2) the tensile properties are strongly correlated with the network draw ratio. As the network draw ratio of the fiber increases, the initial modulus increases, and the network draw ratio has shown better correlation with the initial modulus than with the birefringence. The aggregate model was shown to be effective for estimation of the initial modulus and, especially, the Reuss average gives a good approximation in the case when network draw ratio is used to obtain the orientation parameters. On the other hand, a simple formula was proposed to express the relationship between the initial modulus and the network draw ratio theoretically, based on the intrinsic network structure model, and it has been revealed to show a good agreement with measured data. Yield stress also increases with increase in the network draw ratio and the yield point can be considered as the point on the master curve at the λ_{net}^0 of the sample. It was shown that the breaking takes place before the network structure of the fiber is extended up to the network draw ratio of 10, which corresponds to the ratio of the chain length to the size of the coiled Gauss chain, and true stress at the breaking point is roughly 0.8 GPa, irrespective of molecular orientation and crystallinity. The true stress–strain curve in which σ values are plotted against $\lambda_{net}^2 - 1/\lambda_{net}$ has revealed that PET fibers behave as an ideal rubber in the tensile testing after the yield point. The network structure before the yield point is different from after that but its extension is also affected by network draw ratio. It was also shown that this type of true stress–strain curve provides a new method to estimate the network draw ratio of the sample even if the sample with known λ_{net}^0 is not given. All the results indicate that PET fiber is constituted of the intrinsic network structure and the mechanical properties are determined by the extension of the network structure, i.e., network draw ratio.

One of authors (H. S.) sincerely thanks Prof. I. M. Ward and Dr. A. P. Unwin, University of Leeds, for leading him to the concept of network draw ratio and kind advice to this study.

REFERENCES

1. I. M. Ward, *J. Macromol. Sci.-Phys. B,* **1**(4), 667 (1967).
2. V. B. Gupta and S. Kumar, *J. Appl. Polym. Sci.,* **26,** 1897 (1981).
3. V. B. Gupta and J. Radhakrishnan, *Indian J. Fiber Text Res.,* **16,** 100 (1991).
4. P. B. Rim and C. J. Nelson, *J. Appl. Polym. Sci.,* **42,** 1807 (1991).

5. S. D. Long and I. M. Ward, *J. Appl. Polym. Sci.,* **42,** 1911 (1991).
6. S. D. Long and I. M. Ward, *J. Appl. Polym. Sci.,* **42,** 1921 (1991).
7. W. O. Statton, *J. Appl. Polym. Sci.,* **7,** 803 (1963).
8. Y. Mitsuishi and M. Ikeda, *Kobunshi-Kagaku,* **23,** 319 (1966).
9. I. M. Ward, *Polym. Eng. Sci.,* **24,** 724 (1984).
10. S. W. Allison and I. M. Ward, *Br. J. Appl. Phys.,* **18,** 1151 (1967).
11. H. Brody, *J. Macromol. Sci. Phys. B,* **22**(1), 19 (1983).
12. H. Brody, *J. Macromol. Sci. Phys. B,* **22**(3), 407 (1983).
13. H. Shirataki, A. P. Unwin, and I. M. Ward, to appear.
14. I. M. Ward, *Mechanical Properties of Solid Polymers,* 2nd ed., Wiley, New York, 1990.
15. I. M. Ward, *Proc. Phys. Soc.,* **80,** 1176 (1962).
16. I. M. Ward, *Br. J. Appl. Phys.,* **18,** 1165 (1967).
17. D. W. Hadley, P. R. Pinnock, and I. M. Ward, *J. Mater. Sci.,* **4,** 152 (1969).
18. J. Sweeney and I. M. Ward, *Trans. Inst. Chem. Eng. A,* **71,** 232 (1993).
19. J. Sweeney and I. M. Ward, *Polymer,* **36,** 299 (1995).
20. R. C. Ball, M. Doi, S. F. Edwards, and M. Warner, *Polymer,* **22,** 1010 (1981).
21. S. F. Edwards and Th. Vilgis, *Polymer,* **27,** 483 (1986).
22. F. Rietsch, R. A. Duckett, and I. M. Ward, *Polymer,* **20,** 1133 (1979).
23. H. Shirataki, P. L. Carr, and I. M. Ward, to appear.